CHAPTER 6

A facile and simple strategy for the synthesis of label free carbon quantum dots from the latex of *Euphorbia milii* and its peroxidase-mimic activity for the naked eye detection of glutathione in a human blood serum

6.1. Introduction

Glutathione (GSH), a bio-active molecule is a thiol containing tripeptide and composed of three amino acids L-glutamic acid, L-cysteine, and glycine. GSH is the most plentiful non-protein present in mammalian cells, fungi, plants and also in some prokaryotes. It plays a crucial role in various biological activities such as free radical signal transduction, gene regulation and cellular resistance against xenobiotics [Lu (2009), Estrela *et al.* (2006)]. This tri-peptide exists in tissues in both reduced form (GSH) and oxidized form (GSSG) that retain the intracellular redox potential. Any change in the cellular GSH concentration level leads to the numerous disease like liver damage, caducity, detoxification, leucocytes loss, and heart problems [Townsend *et al.* (2003)]. These anomalies forced the researcher to design the novel and efficient probe towards the detection of GSH. Various methods such as mass spectrometry, chromatography, and immunoluminescence have been designed for the GSH detection [Kailasa *et al.* (2012), Zhang *et al.* (1999), Kamidate *et al.* (1996)]. However; the use of a sophisticated instrument, requirement of tedious pretreatment along with the higher cost has limited their ideality in cellular GSH detection.

Now a days, carbon quantum dots (CQDs) has emerged as a potential source of carbon nanomaterials with size ranges between 2 and 10 nm and exhibits fascinating optical properties due to its high quantum confinement effect [Wen *et al.* (2015)]. They were first discovered accidentally by Xu *et al.* group during the purification of single-walled carbon nanotubes in 2004 [Baker *et al.* (2010)]. These materials are the good substitute over the traditional heavy metal containing semiconductor quantum dots owing to their unique physicochemical properties including good biocompatibility, easy functionalization, less

cytotoxicity, wavelength tunable emission, high solubility in water, high photostability, and robust photobleaching [Lin *et al.* (2015)]. Encouraged by these properties, strategy towards the production of elevated quality CQDs has been paying considerable attention for their wide range of potential application in the field of drug delivery, bio-imaging, photo-catalysis, solar cells, light emitting diodes, wound dressing, catalysis, and sensing applications[Shen *et al.* (2009), Sun *et al.* (2012)]. Usually, these materials have been prepare through oxidization, exfoliation, cutting big size carbon precursors such as carbon nanotubes, graphene oxide, and fullerene into the nano-sized by using different techniques counting laser ablation, chemical oxidation, electrochemical oxidation, pyrolysis, hot injection, hydrothermal, and microwave irradiation [Zhou *et al.* (2007), Zhu *et al.* (2009), Huang *et al.* (2014)]. However; in these synthesis processes except hydrothermal suffer from the use of sophisticated instruments, necessitate of concentrated acids, and uncontrollable reaction circumstances. The hydrothermal route is preferred considerably due to its simple, fast, and efficient process. Numerous organic reagent and polymeric moieties have been recurrently using for the synthesis and surface passivation of CQDs respectively [Shen *et al.* (2011)]. Nevertheless, the use of organic reagents, harsh reaction conditions, and post surface passivation have limited the potential application of CQDs. Hence considering all these factors, researchers are finding an alternative and eco-friendly route regarding environmental concerns to obtain nanomaterials by the utilizing some green precursors. Earlier several researchers have reported the green synthesis of CQDs using natural precursors such as soya bean, orange peels, cotton, cocoon silk, rice husk, peanut shells, seeds and so on [We *et al.* (2015), Li *et al.* (2013), Sahu *et al.* (2012), Pandey *et al.* (2014), Ma *et al.* (2017), Xue *et al.* (2015)].

Peroxidase enzyme is a class of natural enzyme which catalyzes many oxidation-reduction reactions in the analytical diagnosis associated with hydrogen peroxide. However; the use of expensive processes, low stability, the risk of denaturation, and high storage condition restricted its ideality in the analytical diagnosis and encouraged the researcher to develop the artificial enzyme compare with the catalytic properties of peroxidase enzyme. Few literatures are reported on the development of artificial enzyme as the mimetic activity of peroxidase enzyme. Jv *et al.* have synthesized a metal nano-particle possessed a peroxidase mimetic activity for the detection of H_2O_2 and glucose [Jv *et al.* (2010)], Wang *et al.* have designed a supramolecular hydrogel encapsulated hemin as an artificial enzyme to mimic peroxidase [Wang *et al.* (2007)], and Gao *et al.* reported metal oxide framework based peroxidase mimic activity for the detection of H_2O_2 and ascorbic acid [Gao *et al.* (2017). However; metal and costly chemicals used in these synthesis processes restrict their potential applications in analytical and clinical diagnosis.

Herein; we have developed a green approach for the production of biocompatible CQDs using latex of the *Euphorbia milii* (*E. milii)* plant through a facile single-step hydrothermal method involving a polymerization, dehydration, and carbonization cycle. *E. milii* is a common medicinal flowering plant; exude milky white latex at each cut and commonly known as "Christ thrown" in Brazil and other tropical countries [de Matos *et al.* (2011). Latex is generally a complex emulsion that contain proteins, starches, alkaloids, sugars, and gums which are plenteous with the carbon, oxygen, nitrogen, and sulfur source [Lynn *et al.* (1997)]. The proposed methodology avoid the use of metal contamination and concentrated acids and involve the use of green carbon, oxygen, nitrogen, and sulfur containing precursors. It is completely zero-cost having fast reaction rate which require

ultrapure water as the green solvent and avoid the use of other post surface passivating agents. Furthermore, the obtained CQDs served as an intrinsic peroxidase-mimic activity towards the oxidation of TMB and produced a blue colored reaction associated with H_2O_2 which was used as a probe for the GSH detection

6.2. Materials and method

6.2.1. Preparation of CQDs

Typically, 500 μL latexes were collected from the *E. milii* plant and dissolved in 100 mL of ultrapure water and ultrasonicated for 15 minutes in a beaker. Thereafter, the obtained suspended solution was poured into the 250 mL of the Teflon-lined autoclave and heated at 180 ^oC for 3 hours. Now the mixture was cooled down to room temperature. Thus obtained brown carbonaceous material was centrifuged at 14,000 rpm to remove the larger particles for 20 minutes, and the supernatant was pipette out. The obtained light brown supernatant solution was purified against the dialysis membrane for 24 hours. The concentration of purified CQDs was attuned to 0.5 mg/mL and kept in an incubator at 4 ^oC for further use.

6.2.2. Quantum yield determination

The quantum yield of the synthesized CQDs was measured in reference to quinine sulphate from the given **equation 2.3** mentioned in **chapter 2** in a **section 2.6.1**.

6.2.3. Peroxidase-mimic catalytic activity of CQDs

The peroxidase-mimic activity of the as-prepared green synthesized CQDs was determined by measuring the formation of a blue color oxidized product of TMB in the presence of H_2O_2 at 652 nm using the UV-visible spectrophotometer. The proposed reaction was conducted in

a 300 μL of sodium acetate buffer (Na-Ac) (0.2 M, pH 4), 50 μL TMB concentration (2 mM), 50 μL of H_2O_2 concentration (2 mM) catalyzed by the 50 μL of the prepared CQDs (0.5 mg/mL).

6.2.4. Hydroxyl radical detection

The produced $^{\bullet}OH$ radical from the H_2O_2 decomposition in the presence of CQDs were investigated through the fluorescence emission spectra of terephthalic acid because it reacts with $^{\bullet}OH$ radical and forms a fluorescent molecule 2-hydroxyterephthalic acid which exhibits characteristic fluorescence emission intensity around 430 nm. Typically, 0.1 M terephthalic acid solution was prepared in 8 mL of 0.01 M NaOH solution. Thereafter, the different amount of as-prepared CQDs solution 20-80 μL were added into a 2 mL Na-Ac buffer followed by the addition of 50 μL H_2O_2 and 100 μL of terephthalic solution at pH 4, and corresponding fluorescence emission spectra were recorded at an excitation wavelength of 320 nm.

6.2.5. Detection of Glutathione

For the detection of GSH, the different concentrations of GSH were prepared by simple dilution technique using a stock solution of GSH. The GSH detection was carried out by adding 50 μL of TMB (7 mM), and 50 μL of H_2O_2 (8 mM) in a 300 μL of Na-Ac buffer (0.2 M, pH 4) followed by 50 μL of the as-prepared CQDs (0.5 mg/mL). Further, the mixture was kept in the dark for 25 min. Thereafter, 100 μL of the calculated concentration of GSH was added into the TMB+H_2O_2+CQDs reaction system and corresponding absorbance spectra were recorded after the reaction intended for 5 min.

6.2.6. Experimental methodology

The prepared CQDs were characterized through various spectroscopic techniques. The absorbance spectra were measured by a UV-visible spectrophotometer (Thermo Scientific, Evolution 301). The fluorescence spectra were analyzed by the Varian Cary Eclipse Fluorescence Spectrophotometer. Transmission Electron Microscopy micrograph was collected from the TEM, TECHNAI G^2 20 S–TWIN. Zeta potential was measured by NanoPlus HD. The X-Ray Diffraction (XRD) spectrum was collected from the Rigaku MiniFlex 600, at a scanning rate of 3° min^{-1}. The evolved functional groups were explored by the use of Fourier Transform Infrared (FTIR) Spectrum conducted by the FTIR, Perkin Elmer Spectrum 100. X-Ray Photoelectron Spectroscopy (XPS) was conducted by the X-Ray Photoelectron Spectrophotometer (XPS, AMICUS, Kratos Analytical, A Shimadzu).

6.3. Results and discussion

6.3.1. Characterizations

The CQDs were prepared by using green, simple, single-step hydrothermal treatment of *latexes* of *E. milii* plant for 3 hours at 180 ^oC as shown in **Scheme 6.1**.

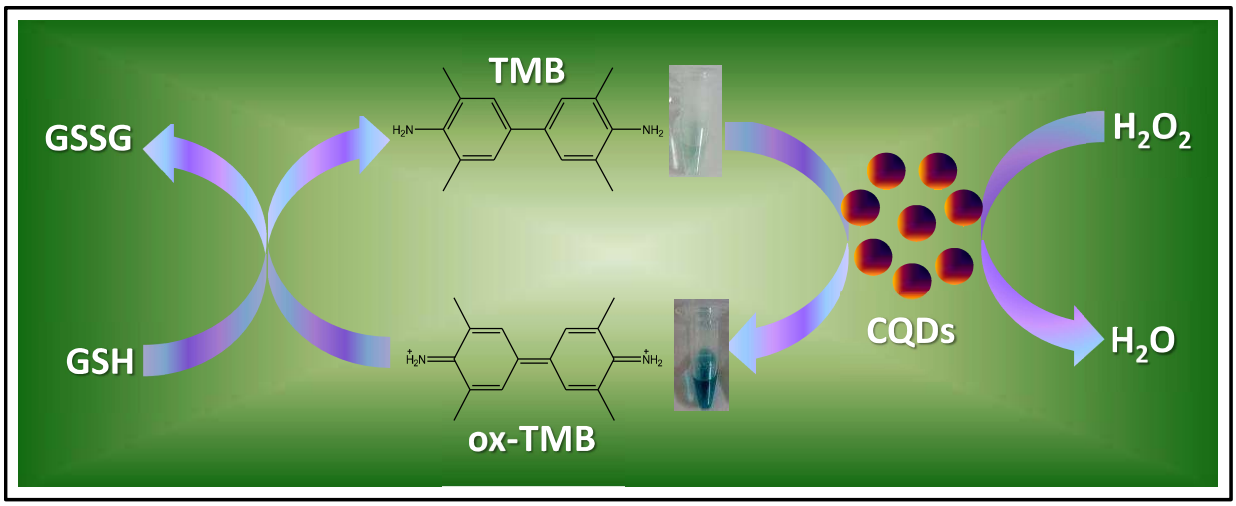

Scheme 6.1 An illustration of peroxidase-mimic activity of the as-prepared green synthesized CQDs for the detection of glutathione.

The size and morphology of the prepared CQDs were confirmed by the TEM micrographs. **Figure 6.1a** clearly revealed the presence of spherical nanoparticles whereas inset showed the particle size distribution with an average diameter of 3.4 ± 0.45 nm. **Figure 6.1b** showed the SAED micrograph of the as-prepared CQDs; the broad circular rings confirmed that the as-prepared CQDs were amorphous in nature. The inset of **Figure 6.1b** presented the HRTEM micrograph at 10 nm magnification which showed that the particles were well dispersed. **Figure 6.1c** explored the crystallinity of the as-prepared CQDs. The broad XRD peak at $2\theta = 23^{o}$, attributed to the 002 Bragg reflections and the corresponding interlayer spacing along with this plane was equal to 0.32 nm which was comparable with the graphite interplanar spacing. This result corroborated the amorphous and graphitic nature of the as-prepared CQDs [Baker *et al.* (2010)]. FTIR analysis before and after formation of CQDs was carried out. The FTIR spectrum of CQDs was different from the precursor which

suggested the formation of CQDs (**Figure 6.1d**). The FTIR spectrum of CQDs showed the peak at 3400 cm^{-1} which was due to the O-H/N-H stretching whereas the peaks at 2859 cm^{-1}, 2916 cm^{-1}, and 1727 cm^{-1} were assigned to the C=C–H, C–C–H, and C=O stretching vibrations respectively. However; the peaks at 1622 cm^{-1} was due to the presence of conjugated O=C–NH in a heterocyclic ring. The characteristic peaks at 1070 cm^{-1} and 1405 cm^{-1} were ascribed to the existence of bending and stretching vibrations of N-H moieties whereas the band at 1250 cm^{-1} resembled to the C–O stretching frequencies [Lu *et al.* (2016)]. The weak band at 630 cm^{-1} and 535 cm^{-1} were due to the C–S stretching mode of vibrations [Rao *et al.* (1964)]. This result indicated that as-prepared CQDs were abundance with the carbon, oxygen, nitrogen, and sulfur moieties.

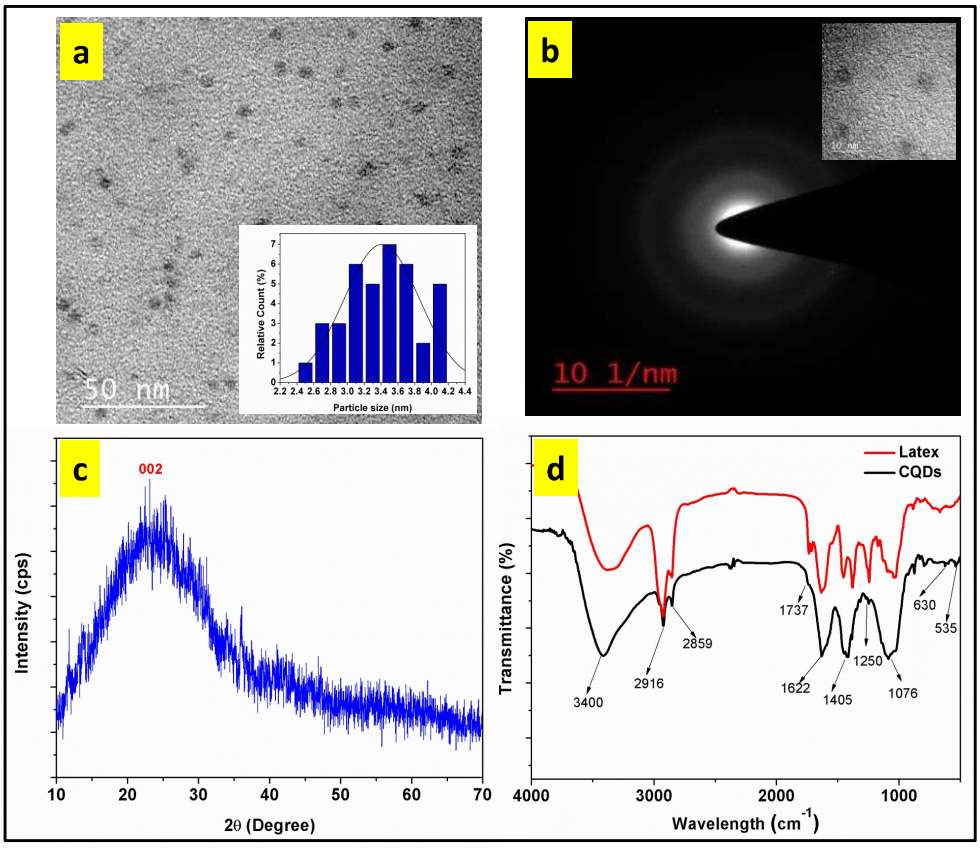

Figure 6.1 (a) Shows the TEM micrograph of CQDs whereas inset elucidate the particle size distribution on counting 45 particles, (b) represents the SAED micrograph of the CQDs and inset shows the HRTEM micrograph at 10 nm magnification, (c) demonstrates the XRD spectrum of CQDs in a range 10-70º with a scan rate 3º/min, and (d) shows the FTIR spectra of CQDs before and after formation.

The elemental composition and bond present on the CQDs surface were analyzed by XPS. The wide scan spectrum of CQDs showed the peaks at 285 eV, 532 eV, 400 eV, and 163.5 eV which confirmed that C, O, N, and S are the main constituent of the as-prepared

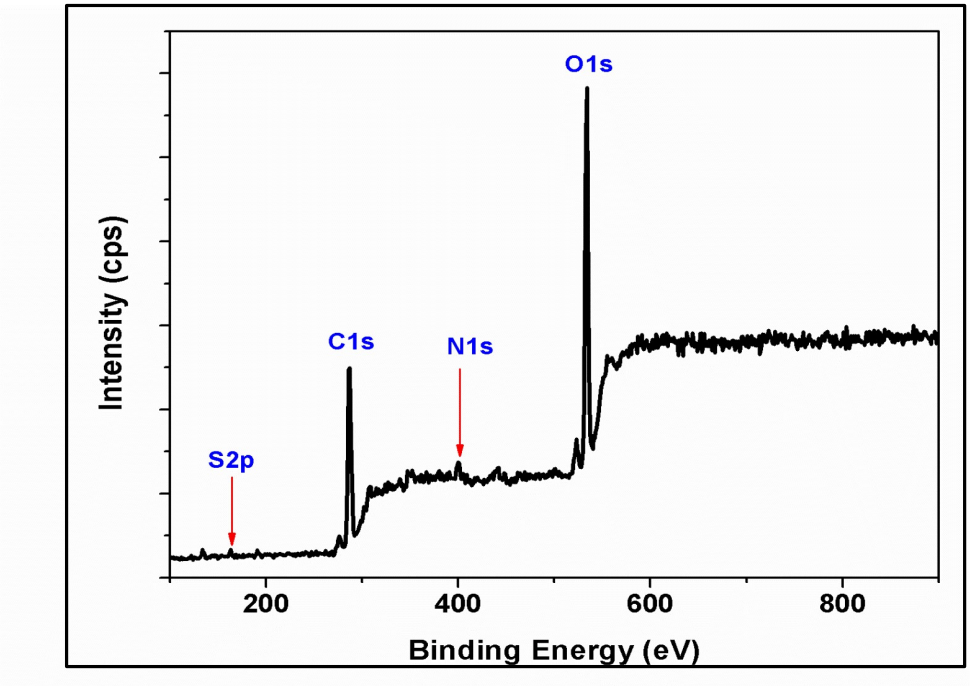

Figure 6.2 Represents the wide scan spectrum of the as-prepared CQDs.

CQDs (**Figure 6.2**). The C1s spectra of CQDs deconvoluted into four peaks at 284.8 eV, 285.7 eV, 286.5 eV, 287.5 eV, and 288.7 eV which were assigned to the occurrence of C–C/C=C, C–OH, C–S, C=O and O–C=O respectively (**Figure 6.3a**) [Lu *et al.* (2017)]. The N1s spectra of CQDs showed the three peaks at 399.9 eV, 401 eV, and 402 eV which were due to the existence of C-N-C, N-C_3, and N-H bonds respectively (**Figure 6.3b**) [Bano *et al.* (2018)]. The O1s spectra explored the peaks at 532.3 eV, 533.4 eV and 534.4 eV which revealed the existence of C=O, C–OH/C–O–C, and O=C–OH, respectively (**Figure 6.3c**). A close look of S2p spectra displayed the peaks at 163.5 eV and 163.4 eV which were due to the presence of C-SH and C-S-C respectively in a CQDs structure (**Figure 6.3d**) [Li *et al.*

(2014), Chaudhari *et al.* (2014)]. These outcomes were consistent with the result obtained from the FTIR analysis which explored the presence of amide, carboxylic, and hydroxyl groups in a prepared CQDs structure.

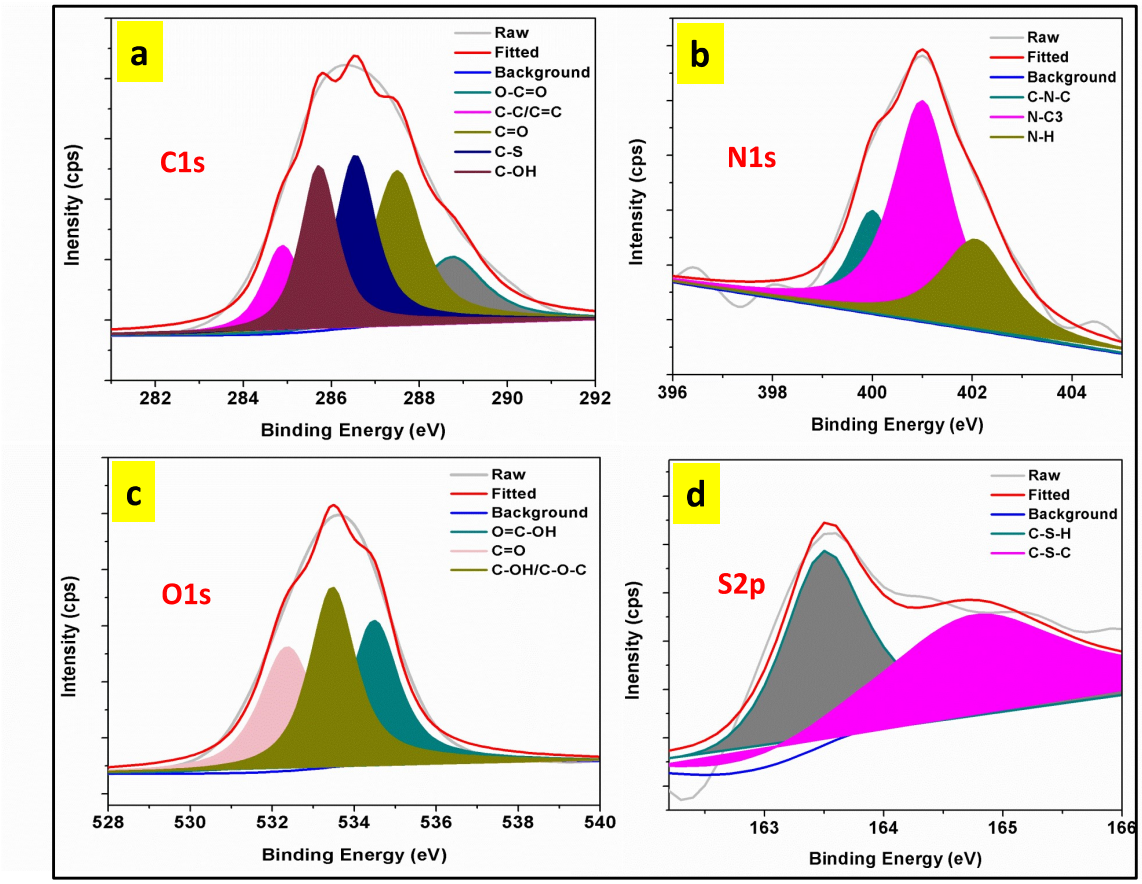

Figure 6.3 (a) High resolution XPS scan of C1s, (b) N1s, (c) O1s, and (d) S2p spectra of the as-prepared CQDs.

6.3.2. Optical Properties

Further, for the future application in bio-imaging, bio-sensors, and other analytical application the optical properties of the as-prepared CQDs were explored. **Figure 6.4a** presented the UV-visible absorption spectrum (black line) and the fluorescence emission spectrum (blue line) of the as-prepared CQDs. The UV-visible spectrum displayed the peaks

at 250 nm and 320 nm which were due to the presence of π-π* (C=C) and n-π* (C=O/C=N) transition respectively with a tails lengthen in a visible region whereas the emission spectrum of CQDs showed the strong peak at 450 nm at the excitation wavelength of 360 nm [Lu *et al*. (2017)]. The inset of **Figure 6.4a** showed that the prepared CQDs exhibited blue emission under the 365 nm excitation in a UV chamber. In previous literature, it was reported that the blue emission of the prepared CQDs was due to the isolated sp^2 nano cluster along with size less than 10 nm yield a band gap consistent with the blue emission in a carbon-oxygen matrix [Eda *et al.* (2010)]. Consequently, in addition to the size and surface, the blue shift was observed due to the presence of oxygen rich species, more electron withdrawing nitrogen atom and occurrence of sulfur in a CQDs structure. The as-prepared CQDs have a relatively high quantum yield (QY) up to 39.2 % with respect to the quinine sulfate as a reference according to the equation 2.1 given in Chapter 2. The FTIR and XPS analysis supported the photoluminescent and relatively high QY of the prepared CQDs. The presence of heteroatom nitrogen and sulfur in the prepared CQDs improve the intrinsic state emission by suppressing the non-radiative electron-hole recombination leading to the photoluminescence and high QY of CQDs [Zhu *et al.* (2012)]. **Figure 6.4b** showed that the prepared CQDs displayed the excitation dependent behavior in the range 280─420 nm with a peak shifted towards the longer wavelength. The red shift may be due to the optical selection of differently sized particles or different emissive traps on the CQDs surface [Wang *et al.* (2014)].

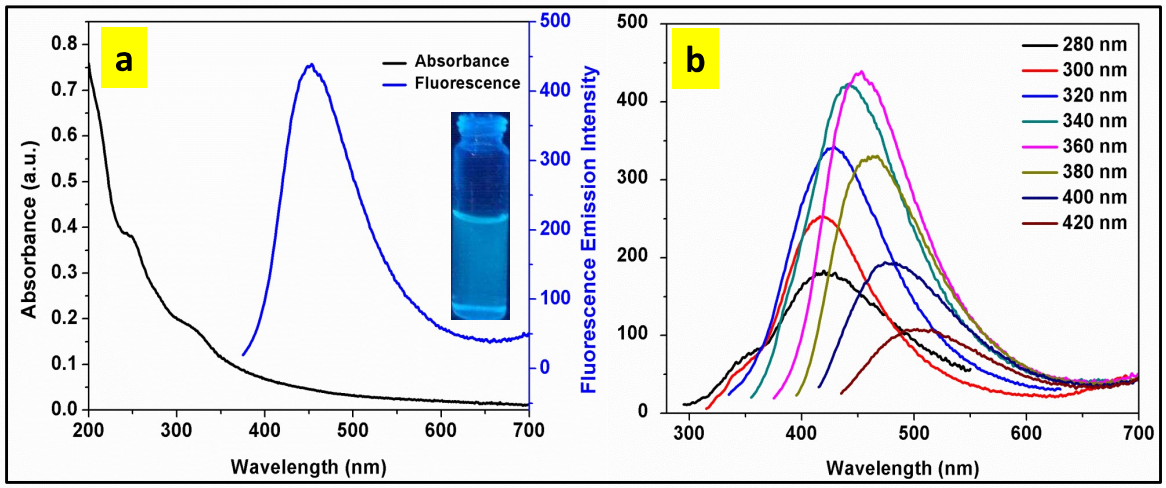

Figure 6.4 (a) UV-visible spectrum (black line) and fluorescence emission spectrum (blue line) at λex 360 nm while inset shows the photograph of vial under UV-excitation at 365 nm in a UV-chamber and (b) shows the fluorescence emission at different excitation wavelength (280, 300, 320, 340, 360, 380, 400, and 420 nm).

As shown in **Figure 6.5a**, the pH stability of the prepared CQDs was investigated in highly acidic and alkaline medium. With the increase of pH from 2 to 7, emission intensity at 450 nm was gradually increased and up to this pH a very slight change was occurred. This phenomenon ascribed to the fact that in a highly acidic medium, the protonation of a carboxyl group on the CQDs surface caused aggregation and leads to the fluorescence quenching [Liu *et al.* (2017). **Figure 6.5b** explored the fluorescence stability of the prepared CQDs in a highly concentrated NaCl salt. The fluorescence emission intensity of CQDs remains unchanged at the varying concentration of NaCl salt solution from 20 to 100 mM. This result confirms that the prepared CQDs was not ionisable and resist the high ionic strength. The photo-stability of CQDs was also checked after illuminating the CQDs under continuous exposure of UV light for 24 hours.

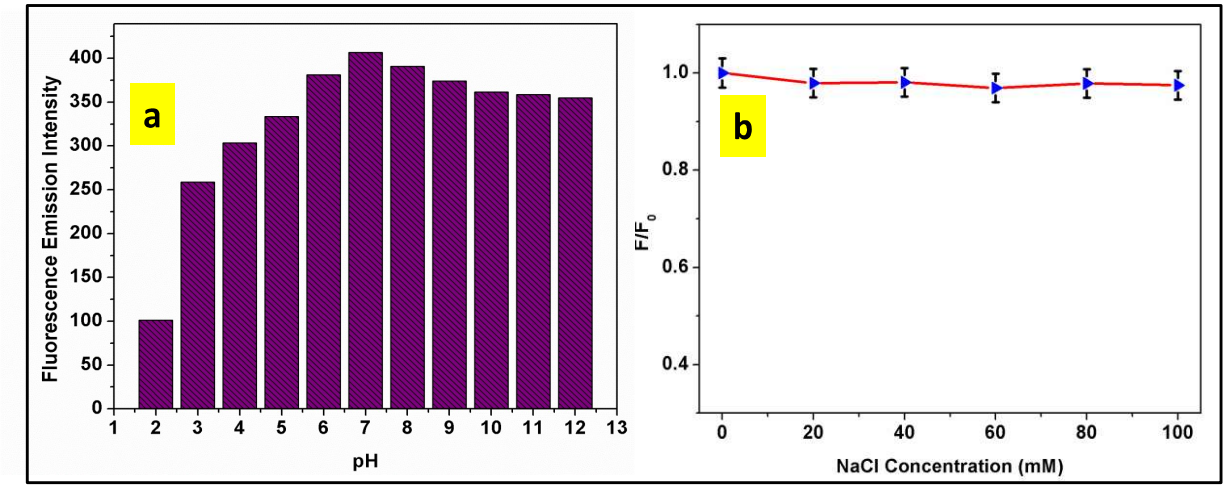

Figure 6.5 (a) Effect on the fluorescence emission intensity on varying pH from 2 to 12 (b) ratio of fluorescence intensity after incubating NaCl concentration (0-100 mM), where F is the fluorescence emission intensity at 450 nm after incubating NaCl salt solution and F_0 denotes the fluorescence emission intensity before the addition.

As shown in **Figure 6.6a**, a very small fluorescence emission change was occurred after illuminating the UV light for 24 hours indicating the high photostability of CQDs. Besides, the stability of the as-prepared CQDs was also checked over the months as shown in **Figure 6.6b**. A very negligible change was observed in fluorescence emission of CQDs even after 4 months of incubation at 4 ^{o}C; this observation demonstrated the high stability of the as-prepared CQDs at ambient condition. A high zeta potential value around -8.47 mV suggested that the prepared CQDs were highly dispersed in water (Fig. 4.6c). The hydrophilicity of the prepared CQDs was further explored by the use of like-dissolves-like technique (**Figure 6.6d)**. The addition of the prepared CQDs into the mixture of the certain classic solvents with water such as dichloromethane, chloroform, and hexane respectively

confirms that the as-prepared CQDs were prominently dispersed in water and exhibited the blue emission at the excitation wavelength of 365 nm in a UV-chamber.

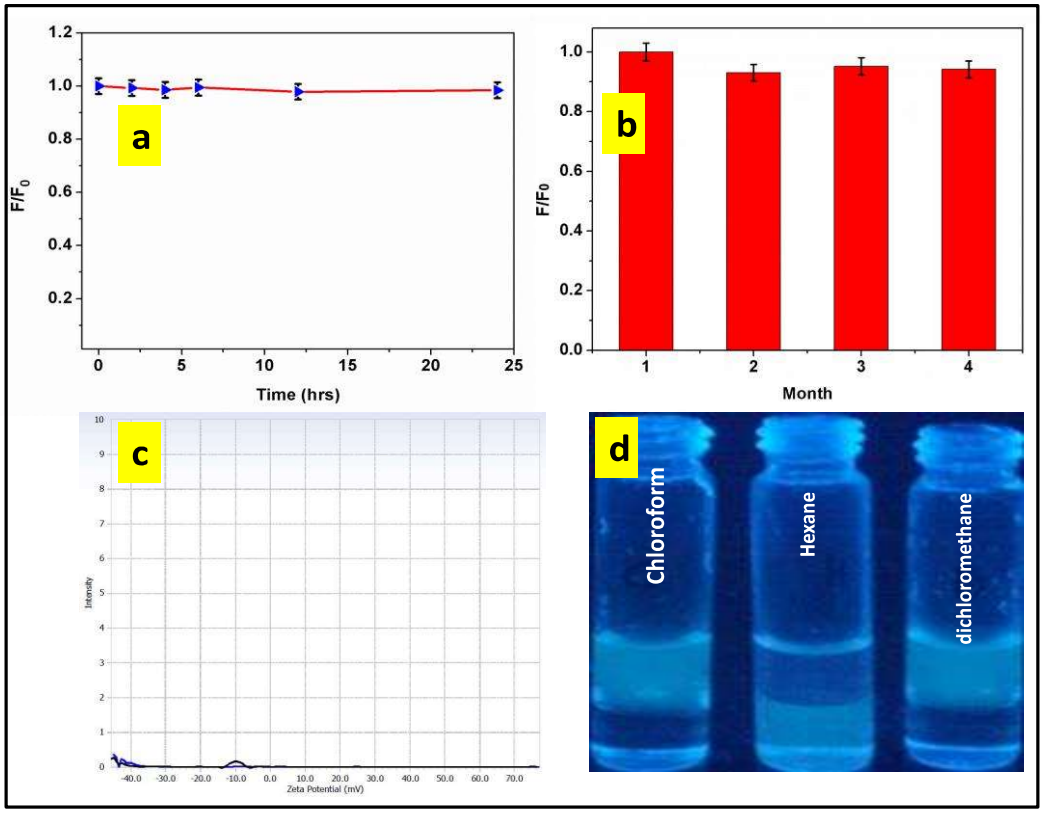

Figure 6.6 (a) Shows the effect of fluorescence emission after exposing UV light for 24 hrs, (b) explores the fluorescence stability over 4 months of incubation, (c) Shows the scanned Zeta potential image of the as-prepared CQDs, (d) express the hydrophilicity of the CQDs in a mixture of water with certain classic solvent. Error bar shows the three independent repeated measurements.

Thus, the as-prepared CQDs showed the excellent optical properties which could be potentially applied in the field of bio-imaging, bio-sensors, and several other analytical applications.

6.3.3. Study of peroxidase-mimic activity of the green synthesized CQDs

The as-prepared CQDs catalyzed the peroxidase substrate TMB speedily in the presence of H_2O_2 and produced the colored reaction from colorless to blue along with the characteristics absorbance peak at 652 nm which was used for the GSH detection. Here TMB substrate was taken as an indicator which produced the blue color of oxidized TMB (ox-TMB). Furthermore, the addition of GSH into the optimized TMB+H_2O_2+CQDs reaction system faded the color of the reaction system from blue to transparent and corresponding absorbance spectra also decreased gradually.

Figure 6.7a showed the characteristic UV-visible absorbance spectra of TMB, TMB+H_2O_2, and TMB+H_2O_2+CQDs reaction system. The absorbance peak of the TMB+H_2O_2+CQDs reaction system at 652 nm was much higher compared to that of TMB and TMB+ H_2O_2 reaction systems. This result confirmed that the prepared CQDs behaved as a catalyst towards the oxidation of TMB. **Figure 6.7b** presented the absorbance peak at 652 nm of TMB+CQDs, TMB+H_2O_2, and TMB+H_2O_2+CQDs reactions system with a catalytic time course of 40 min. A very high absorbance change was observed in case of TMB+CQDs+H_2O_2 reaction system as compared to TMB+CQDs and TMB+H_2O_2 which became stable in a broad range from 25 to 40 min. The inset of **Figure 6.7b** showed the typical blue color reaction of peroxidase substrate TMB in the presence of H_2O_2 catalyzed by CQDs. This result explored that CQDs or H_2O_2 alone in a reaction system did not produce any significant blue color and 25 min incubation time was enough for the completion of the reaction.

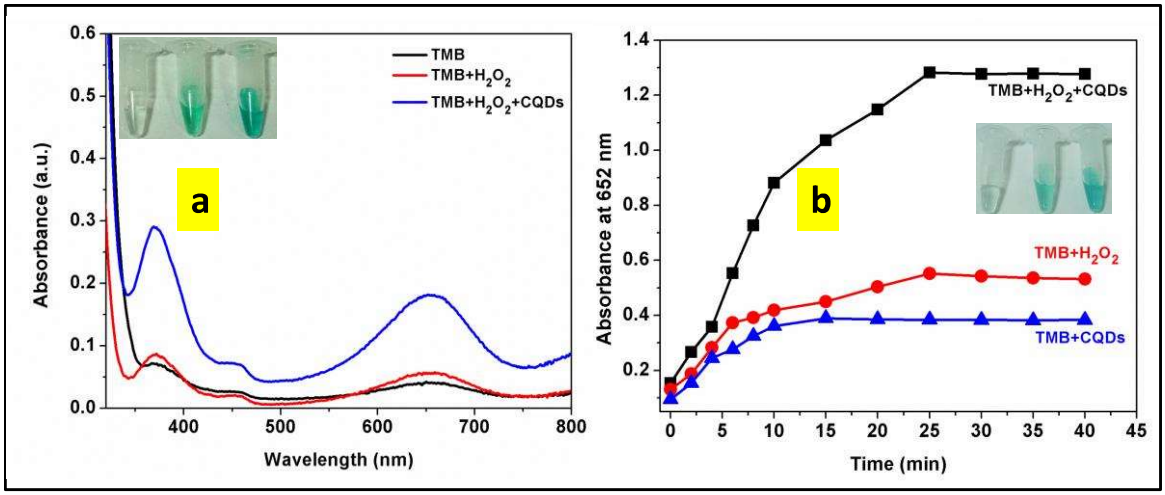

Figure 6.7 (a) Represents the UV-visible absorbance spectra of TMB, TMB+H_2O_2, and TMB+H_2O_2+CQDs reaction system,(b) absorbance changes at 652 nm of ox-TMB with a catalytic time course 40 min in a different reaction system TMB+CQDs, TMB+H_2O_2, and TMB+ H_2O_2+CQDs ([TMB] = [H_2O_2] = 2 mM, [CQDs] = 0.5 mg/mL) whereas inset represents the blue colored reaction of ox-TMB.

In order to get the optimum result for enhanced catalytic performance; pH, temperature, H_2O_2 concentration, and TMB concentration were optimized. The peroxidase-mimic activity of CQDs was investigated at different pH ranged from 2 to 6. From the UV-visible absorbance spectra with a characteristics peak at 652 nm, it was found that the CQDs displayed an excellent peroxidase-mimic activity at pH 4 selectively and beyond this pH, the peroxidase-mimic activity started to decrease (**Figure 6.8a**). This result confirmed that the as-prepared CQDs showed the pH-dependent catalytic ability. The effect of temperature on the peroxidase-mimic activity of CQDs was also investigated at constant pH 4 as shown in **Figure 6.8b**. It was found that the prepared CQDs showed the maximal peroxidase-mimic activity at 40 °C and up to this temperature the peroxidase-mimic activity decreased which owed to the agglomeration of CQDs resultant in the interruption of the electron transfer

process [Feng *et al.* (2017)]. **Figure 6.8c** indicated that on varying the H_2O_2 concentration from 1 to 10 mM, the absorbance spectra of the reaction system centered at 652 nm increased gradually up to the 8 mM and up to this concentration it decreased. After that, TMB concentration was also varied at a fixed H_2O_2 concentration and found that at first, the absorbance peak at 652 nm increased up to 7 mM and beyond this concentration it decreased (**Figure 6.8d)**.

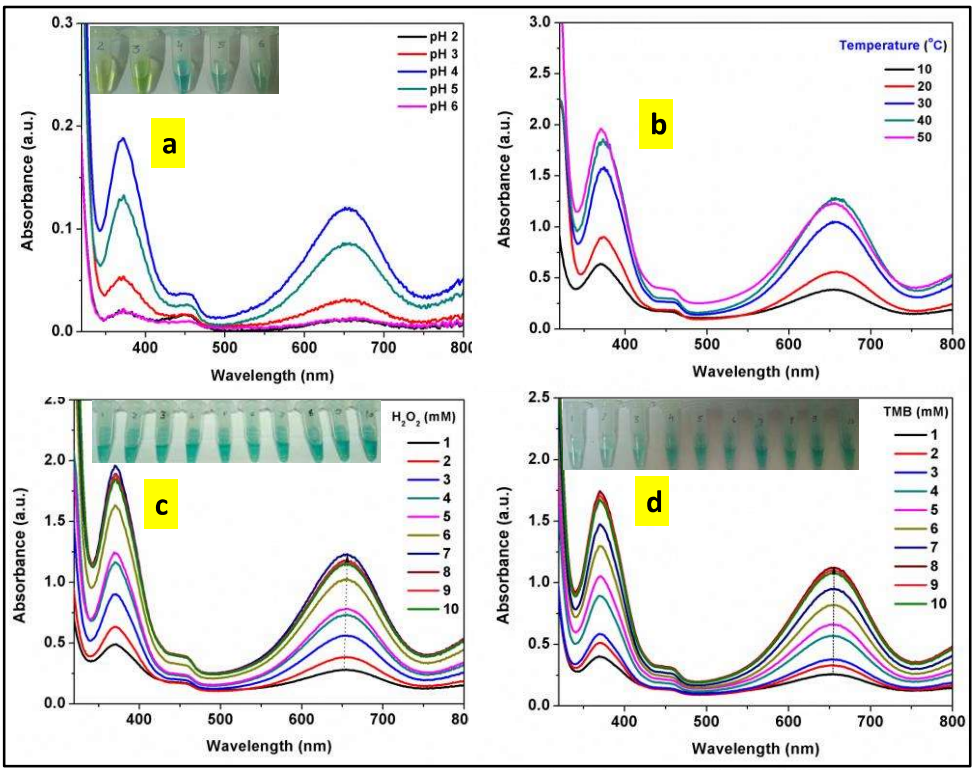

Figure 6.8 (a) Represents the absorbance spectra of TMB based oxidation at different pH ranges from 2 to 6, (b) effect of temperature, (c) optimization of H_2O_2 concentration, and (d) optimization of TMB concentration on the peroxidase-mimic activity of the as-prepared CQDs.

Thus the obtained result concluded the peroxidase-mimic activity of green synthesized CQDs which catalyzed the reaction system of TMB+H_2O_2 and produced the ox-

TMB at an optimum pH 4, temperature 40 ^{o}C, 8 mM of H_2O_2, and 7 mM of TMB concentration.

6.3.3.1. Kinetic studies of the peroxidase-mimic activity

To look into the kinetic mechanism of the peroxidase-mimic activity of the green synthesized CQDs, the steady-state kinetic parameters for the peroxidase-mimic reaction were determined by varying the TMB and H_2O_2 concentrations which was carried out one by one with respect to time in the proposed reaction system. The initial rate of the derived oxidized product was calculated from the absorbance data and the molar absorption coefficient for the TMB derived oxidized products (ε=39,000 $M^{-1}cm^{-1}$) by using Lambert-Beer (**equation 6.1**) law as shown below.

$$\boldsymbol{A = \varepsilon c b} \qquad 6.1$$

Where A is represented as the absorbance, c is denoted as the substrate concentration, and b is for the thickness of the sample. **Figure 6.9a and c** showed the typical Michaelis–Menten curves which were obtained by fixing the H_2O_2 concentration at 8 mM and varying the TMB concentration and in a scheme experiment TMB concentration was fixed at 7 mM and varying the H_2O_2 concentration. From the obtained Michaelis–Menten curves Lineweaver-Burk plot were obtained as shown in **Figure 6.9b and d**.

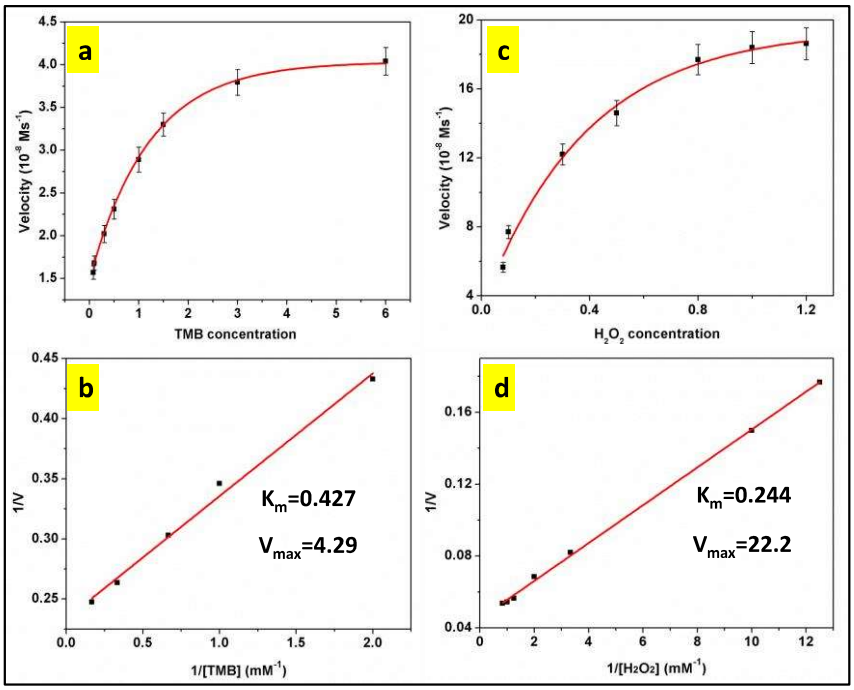

Figure 6.9 Shows the steady state kinetic analysis and catalytic mechanism of CQDs (a-d), error bars represent the standard error on measuring three repeated measurement (a) the H_2O_2 concentration was fixed at 8 mM and TMB concentration was varied from 0.08 to 6 mM whereas (b) shows the lineweaver-burk plot corresponding to fixed H_2O_2 concentration, (c) the TMB concentration was fixed at 7 mM and H_2O_2 concentration was varied from 0.08 to 1.2 mM, and (d) shows the lineweaver-burk plot corresponding to fixed TMB concentration.

The typical Michaelis–Menten constant (K_m) and maximum velocity (V_{max}) was obtained from the **equation 6.2**.

$$\frac{1}{V} = \frac{K_m}{V_{max}} \cdot \frac{1}{[S]} + \frac{1}{V_{max}} \qquad 6.2$$

Where V stands for the initial reaction velocity, V_{max} denotes the maximum initial velocity, K_m is the Michaelis-Menten constant, and [S] represents the substrate concentration. The visible steady state rates at different substrate concentration were observed by calculating the

slopes of the initial absorbance changes with time (absorbance spectrum was performed by one-minute frequency for 5 min). Experimentally, it was found that the catalytic ability depends upon the K_m and V_{max} values. The lesser K_m value derived the stronger attraction amid the enzyme and substrate which confirmed that the as-prepared CQDs behaved as an efficient catalyst. The higher V_{max} value suggested the higher efficiency towards TMB oxidation in the presence of H_2O_2. It was also found that the obtained K_m value towards the catalytic ability of as-prepared CQDs was very low and V_{max} was quite high as compare to the HRP and several other nanomaterials as shown in **Table 6.1**. These result confirmed that the as-prepared green synthesized CQDs performed as an efficient catalyst towards the oxidation of TMB.

Table 6.1 Comparison of the obtained kinetic parameters K_m and V_{max} with other nanomaterial and HRP.

Catalyst	Substrate	K_m (mM)	V_{max} (10^{-8} Ms^{-1})	Ref.
HRP	TMB	0.434	10	[Shi *et al.* (2011)]
	H_2O_2	3.702	8.71	
GQDs	ABTS	10.4	1.78	[Sun *et al.* (2015)]
	H_2O_2	1.17	1.24	
Si-Dot	TMB	1.502	14.72	[Chen *et al.* (2014)]
	H_2O_2	0.065	5.65	
CQDs	TMB	0.427	4.29	[Bano *et al.* (2019)]
	H_2O_2	0.244	22.2	

The nature of peroxidase-mimic activity of the green synthesized CQDs might be due to the ability of H_2O_2 reduction. This is verified by the fluorescence and absorbance spectroscopy of the reaction (**Figure 6.10)**. To confirm this hypothesis, terephthalic acid (TPA) was used as a $^{\bullet}OH$ radical probe because it produces highly fluorescent 2-

hydroxyterephthalic acid (TPAOH) molecule by trigging with •OH which exhibits fluorescence emission at 425 nm upon excitation at 320 nm. The fluorescent spectra of TPA and H_2O_2 solution were carried out in the presence of different concentration of CQDs catalyst at pH 4. From the **Figure 6.10a,** it is clear that emission spectra were increased on increasing the concentration of CQDs from 20 to 80 μL. This result demonstrated that TPA is triggered by •OH radical and produced the fluorescent molecule TPAOH; thus formation of TPAOH was relative to the concentration of the CQDs. This finding confirmed that the green synthesized CQDs generated the •OH by activating H_2O_2 molecule and catalyzed the TMB based oxidation associated with H_2O_2. Furthermore, to confirm the formation of a •OH radical during TMB based oxidation reaction in the presence of H_2O_2 catalyzed by CQDs, a control experiment was also performed. Methyl alcohol (MA), thiourea (TU), isopropyl alcohol (IPA), and dimethyl sulfoxide (DMSO) was chosen as a •OH radical scavenger and added into the TMB+H_2O_2+CQDs system and UV-visible spectra were monitored out. As shown in **Figure 6.10b**, the absorbance peak at 652 nm decreased in the presence of •OH scavenger which was due to the partial oxidation of TMB. The decrease in absorbance at 652 nm indicated the presence of •OH radical in TMB based oxidation reaction. The above result concluded that •OH was generated by the reduction of H_2O_2 and released H_2O; this radical oxidized the TMB and resulted into the formation of typical blue color oxidized product [Breslow (1995)].

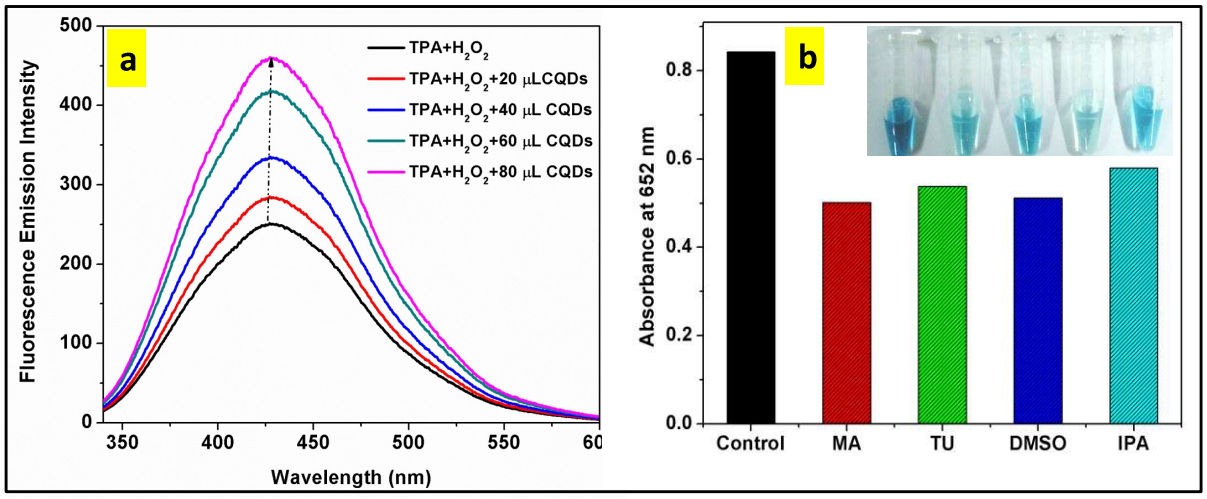

Figure 6.10 (a) Shows the fluorescence emission spectra of TPAOH formed from the oxidation of TPA by ˙OH radical which was generated during the destruction of H_2O_2 on activating with CQDs and (b) shows the effect of ˙OH radical scavenger on the peroxidase-mimic activity of CQDs.

On the basis of the above result, it was supposed that high surface area and small size of the as-prepared CQDs may lead to facilitate the more number of ˙OH radical. Moreover, positively charged TMB was absorbed on the negatively charged CQDs surface and mediated the electron transfer to the green synthesized CQDs from NH_2 group of TMB. This leads to the electron density enhancement on the CQDs surface and accelerated the H_2O_2 reduction into ˙OH which assisted the oxidation of TMB along with reaction color change from transparent to blue [Breslow (1995)]. Thus the as-prepared CQDs showed the excellent peroxidase-mimic activity without any use of other foreign materials.

6.3.4. Assay towards the detection of glutathione

The proposed CQDs based catalyzed system of TMB (7 mM), H_2O_2 (8 mM), and CQDs (0.5 mg/mL) acted as a probe towards the detection of bio-active GSH molecule by

fading the color of the reaction from blue to transparent which can be easily seen by our naked eye. The selectivity of the present sensing towards the detection of GSH was evaluated after adding 100 μL (100 μM) of each glycine (Gly), proline (Pro), phenylalanine (Phe), asparagine (Asprg), serine (Ser), threonine (Thr), tryptophan (Try), tyrosine (Tyr), leucine (Leu), alanine (Ala), aspartic acid (Asp), valine (Val), cysteine (Cys), glucose (Gluc), methionine (Met), ascorbic acid (AA), uric acid (UA), citric acid (CA), and tartaric acid (TA) as an interference into the TMB+H_2O_2+CQDs reaction system and corresponding absorbance at 652 nm were recorded. **Figure 6.11** showed the change in absorbance (ΔA) at 652 nm after the addition of different amino acids and various other interfering agents into the TMB+H_2O_2+CQDs reaction system whereas inset showed the photographs of observed blue color during the selectivity experiment. It was found that ΔA was comparatively high in the case of GSH, cysteine, and AA than that of other amino acids and interfering agent. As shown in **Figure 6.11**, a very high absorbance change in the presence of GSH was observed as compared to Cys and AA. This may be due to its high reducing ability towards the ox-TMB as GSH reduced the ox-TMB into the TMB and simultaneously oxidized itself into the GSSG [Ni *et al.* (2015)]. The different reduction ability of the GSH, Cys, and AA may be accredited to the different reducing functional groups present in the studied molecules, such as –OH, O=C–OH, –NH_2, –NH, and –SH. This finding confirmed that the proposed sensing system demonstrated the good selectivity over other amino acids and various other interfering agents towards the detection of GSH.

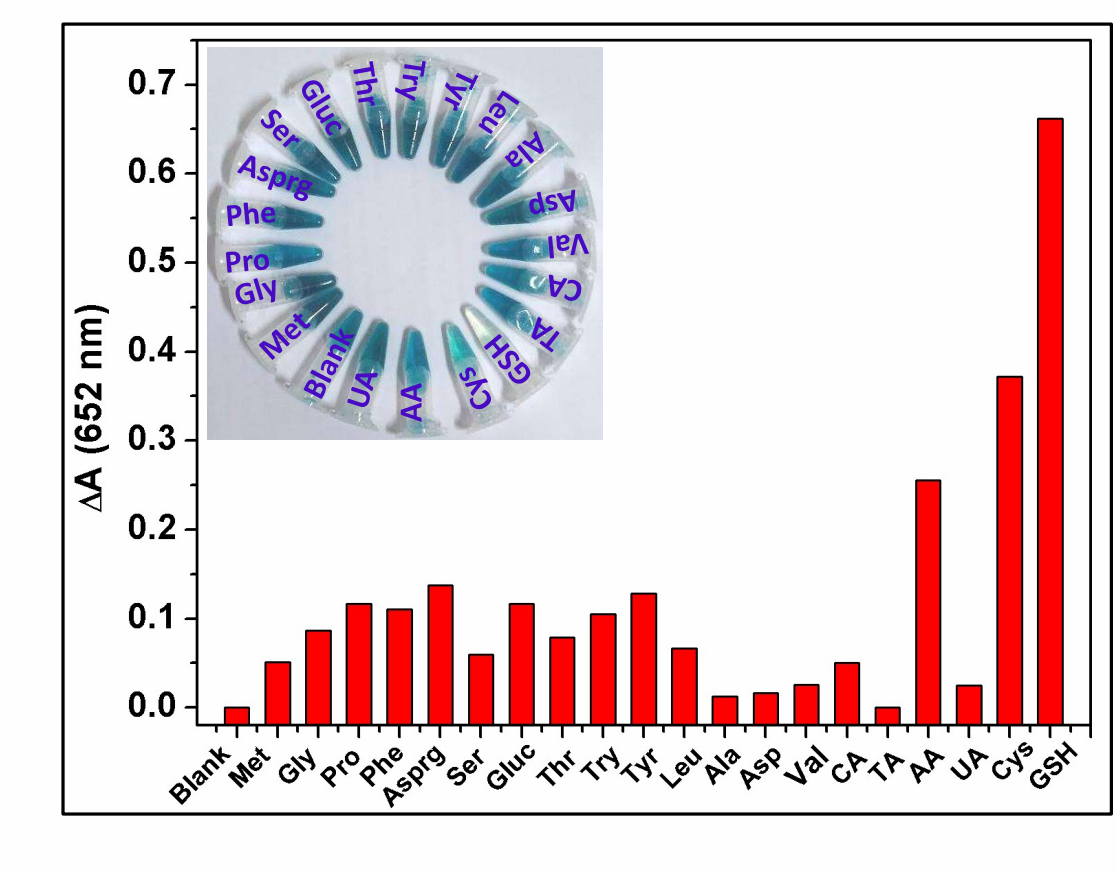

Figure 6.11 Represents the change in absorbance at 652 nm after the addition of different amino acids, GSH, gluc, AA, TA, CA, and UA (100 μM) into the TMB+H_2O_2+CQDs whereas inset shows the corresponding reaction color obtained during the addition ([TMB] = 7 mM, [H_2O_2] = 8 mM, and [CQDs] = 0.5 mg/mL). Where $\Delta A=A_0-A$, A_0 is for the initial absorbance and A for the absorbance obtained after the addition of amino acids, glucose, and GSH.

Beside the selectivity, sensitive titration is another important experiment towards the GSH detection (**Figure 6.12**). As shown in **Figure 6.12a**, on increasing the GSH concentration from 0 to100 μM the absorbance spectra of the ox-TMB decreased whereas inset showed the observed color change from blue to transparent with the increasing GSH concentration. **Figure 6.12b** corroborated the change in absorbance (ΔA) at 652 nm

increased with the increased concentration of GSH upto 80 μM and onwards this very slight change was observed. The inset of **Figure 6.12b** showed the good linearity on increasing the

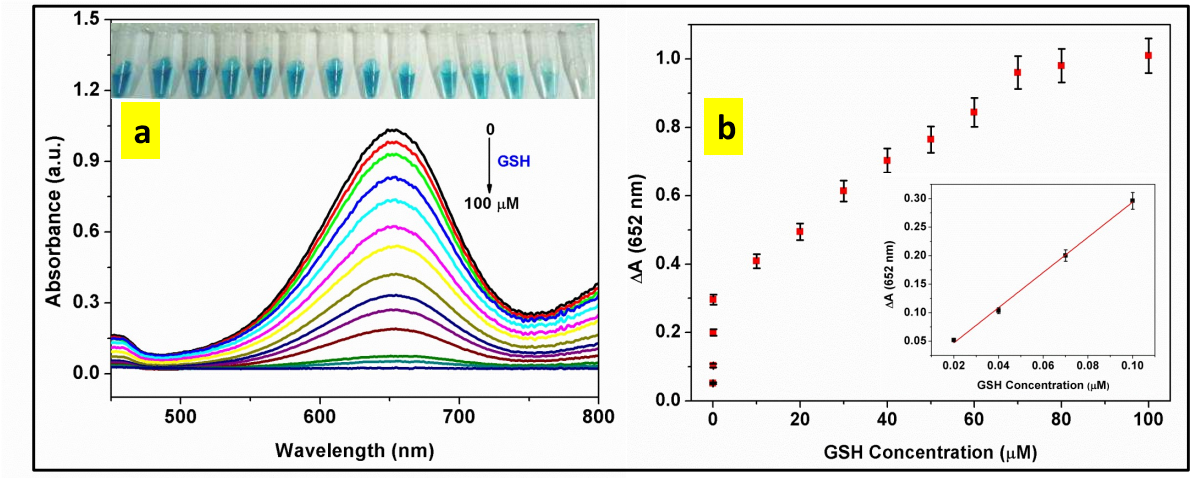

Figure 6.12 (a) Absorbance spectra of ox-TMB on increasing the GSH concentration (0-100 μM), (b) change in absorbance at 652 nm with the increased GSH concentration. Inset figure shows the linear calibration plot for the reduction of ox-TMB in a range 0.02–0.1 μM. Error bars shows the standard error on measuring three repeated measurements.

concentration of GSH from 0.02 to 0.1 μM with a linear equation $\Delta A=3.08[GSH]-0.087$ and $R^2=0.997$. The calculated LOD in this linear range was found to be 5.3 nM which was better than the previously reported literature as shown in **Table 6.2.**

Table 6.2. Sensing performance of different nano-probe for the detection of GSH.

Sensing system	Sensing method	Linear range	LOD	Ref.
g-C_3N_4-MnO_2	Colorimetric	0–2 μM	0.2 μM	[Zhang *et al.* (2014)]
MnO_2-TMB	Colorimetric	0.26–26 μM	0.1 μM	[Liu *et al.* (2013)]
Fe_3O_4-ABTS-H_2O_2	Colorimetric	3.0–30 μM	Not provided	[Ma *et al.* (2012)]
PEI-capped AgNCs	Fluorometric	0.5–6 μM	0.38 μM	[Zhang *et al.* (2013)]
CQDs-AuNPs	Colorimetric	1–4 μM	Not provided	[Shi *et al.* (2014)]
AuNPs	Colorimetric	0.5–1.25 μM	0.5 μM	[Hu *et al.* (2013)]
AuNCs-Hg^{2+}	Fluorometric	0–250 μM	9.4 nM	[Park *et al.* (2013)]
CQDs-TMB	Colorimetric	0.02–0.1 μM	5.3 nM	[Bano *et al.* (2019)]

6.3.4.1. Detection of glutathione in human blood serum

To explore the practical feasibility towards the detection of GSH, the sensing potential of the proposed sensing system was investigated in a natural sample. The efficacy of TMB+H_2O_2+CQDs based sensing system was inspected in the five human blood serum samples which were collected from the Sir Sunder Lal Hospital, Banaras Hindu University, Varanasi, India. The collected blood serum samples were centrifuged up to 12,000 rpm for 15 min and the supernatant were taken out. The obtained serum samples were analyzed before and after spiking with the known concentration of GSH. Before spiking, the found GSH in a serum samples were 15.1 μM, 54.4 μM, 48.3 μM, 35.7 μM, and 23.8 μM. Thereafter, recovery experiments were performed after spiking the serum samples with the different concentration of GSH (5, 10, and 15 μM). The recovered GSH concentrations were in the range of 93.4-102.9 % along with relative standard deviation (RSD) below 5%, as shown in **Table 6.3**. This result advocated the feasibility and reliability of the

TMB+H_2O_2+CQDs based sensing system towards the GSH detection in a clinical sample analysis.

Table 6.3. Detection of GSH in a human blood serum and RSD for the three replicate measurements.

Human Blood Serum	Before spiking GSH found (μM)	After Spiking GSH (μM)	GSH found (μM)	Recovery (%)	RSD (%)
Serum 1	15.1	5	19.3	94.1	1.86
		10	25.4	102	2.58
		15	29.1	93.4	1.57
Serum 2	54.4	5	60.1	101.3	2.09
		10	62.9	97.2	2.46
		15	68.8	98.9	1.98
Serum 3	48.3	5	54.1	101.6	3.10
		10	56.6	96.5	1.47
		15	62.7	98.7	2.34
Serum 4	35.7	5	40.3	98.9	2.25
		10	46.1	101.1	2.44
		15	49.3	96.0	3.36
Serum 5	23.8	5	29.5	102.9	1.01
		10	32.9	96.2	2.93
		15	39.3	102.1	2.68

6.4. Conclusion

In summary, the CQDs is prepared through a simple, green, facile, and single-step hydrothermal treatment by using latex of medicinal plant *E. milii*. The proposed method has many advantages such as there is no use of strong concentrated acid which did not release any toxic gases, use of zero-cost green precursor instead of costly organic carbon precursors which avoided the metal contamination, and ultrapure water as a green solvent. The resultant CQDs displayed excellent optical properties including high QY up to 39.2 %, resisted to high salt strength, and longtime photostability. Furthermore, the prepared CQDs served as an intrinsic peroxidase-mimic for catalyzing the TMB in the presence of H_2O_2 at 652 nm. In addition to this, the proposed TMB based system acted as a probe towards the detection of

GSH with good selectivity in different amino acids and various other interfering agents. The LOD towards the GSH detection was found to be 5.3 nM in a linear range 0.02-0.1 μM which showed superiority to another reported probe. The proposed TMB based sensing system was successfully applied to the human blood serum samples with good recovery 93.4–102.9 % which demonstrated the practical feasibility of the present sensing system.

The present thesis described the development of different type of CQDs based nanoprobe for the detection of metal ions and biosensor. The CQDs were synthesized by the chemical as well as natural organic precursor by the use of simple one-step hydrothermal method. The CQDs were characterized by the various modern techniques such as Fourier Transform Infrared (FTIR) Spectroscopy, UV-visible Spectroscopy, Fluorescence Spectroscopy, X-Ray Diffraction (XRD), Transmission Electron Microscopy (TEM), Energy-Dispersive X-Ray Spectroscopy (EDAX), Selected Area Electron Diffraction Pattern (SAED), and X-Ray Photoelectron Spectroscopy (XPS). Furthermore, these CQDs have been implemented for the sensing applications in the detection of Co(II), Hg(II), and glutathione (GSH). In addition to this, the potential feasibility of the proposed sensing system were also deliberated successfully on the real natural sample analysis.

Chapter 1 The current chapter deals with the exhaustive literature survey related to economical and green route for the CQDs synthesis. This chapter described the various types of nanomaterials, and their synthesis approaches briefly. This chapter also discussed an overview and history of CQDs. The present chapter also discussed the properties and application of CQDs as well as objective of the current thesis work.

Chapter 2 The present chapter furnishes the materials and the protocols used in the present thesis work. This chapter provides the list of chemical which have been used up throughout the experiments. This chapter also covers the detailed procedures of the preparation of CQDs, experimental processes of various applications done in this chapter such as detection of heavy metals Co(II), Hg(II), and bioactive molecule GSH.

Chapter 3 In this work, we have successfully prepared the highly fluorescent N–CQDs by using simple one-step hydrothermal treatment. The size of the synthesized CQDs were

confirmed by the TEM microscopy which revealed that the particles were in the range of 2 to 2.5 nm. EDAX analysis confirmed the prepared N–CQDs were composed of C, O, and N. The broad XRD spectrum at 2θ = 23° along with the facet (002) confirmed the amorphous nature of CQDs. The elemental state, bonding present, and composition were further confirmed by the XPS analyses which were supported by the FTIR analysis. Furthermore, the optical properties of synthesized N-CQDs were also discovered. The synthesized N–CQDs exhibited the strong blue fluorescence at the excitation wavelength of 365 nm under UV light along with CIE co-ordinate index (0.15, 0.14). Moreover, the as-prepared N-CQDs demonstrated very high QY up to 57 % using quinine sulfate as a reference. Apart from this, the prepared N–CQDs are found to be a good nano-probe for the selective and sensitive detection of Co^{2+} with a detection limit of 0.12 μM in a linear range from 0.5 to 3.0 μM. The sensitivity of the detection system is achieved by the quenching mechanism based on the IFE, static quenching, aggregation, and formation of cobalt-amine complex amid the N–CQDs and Co^{2+}. The present sensing system is also successfully applied to the vitamin B-12 sample as the practical application of Co^{2+} detection. We hope that the present work may offer a new move towards the Co^{2+} detection along with other toxic ions having low cost, high sensitivity, and selectivity for the environmental, clinical, and analytical applications.

Chapter 4 In the present chapter, a synthetic approach was developed for the off-on sensing of GSH by using N,S–CQD–MnO_2 nano-composite based nanoprobe. The N,S–CQDs were synthesized via hydrothermal treatment of tartaric acid and taurine precursors. The TEM micrograph revealed that the particle were in the range of 2–3 nm. The chemical composition, surface state and bond present were confirmed by the XPS analysis and consistent with the FTIR analysis. The broad XRD peak at 25° along with (002) reflection

confirmed the amorphous nature of N,S–CQDs. The optical properties of synthesized CQDs were also probed. The synthesized N,S–CQDs exhibited strong blue emission at 365 nm excitation. The measured QY was high up to 47.4 %. Introduction of MnO_2 nanosheets quenched the fluorescence emission of N,S–CQDs by the phenomenon of fluorescence resonance energy transfer and strong electrostatic interactions between them. Furthermore, the MTT assay also confirmed that the as-prepared N,S–CQD–MnO_2 based nanoprobe show very low-cytotoxicity and good biocompatibility. The fluorescence can reappear after the addition of GSH into the nano-composite solution because it triggers the decomposition of MnO_2 nanosheets into Mn^{2+}, which leads to the elimination of fluorescence resonance energy transfer. The calculated detection limit was found to be 0.012 μM in a GSH concentration having a linear range of 0.1–0.7 μM. Thus, based on the fluorescence recovery by GSH, the synthesized nanoprobe possesses high sensitivity with multi interesting features including easy preparation, economic, and less cytotoxicity. Apart from this, the present sensing system is successfully demonstrated good feasibility for *in vitro* imaging GSH in A549 human lung cancer cell. Further, the practicability of the proposed sensing system is also efficaciously applied to human blood serum in quantification of GSH. Such a highly sensitive nanoprobe could be potentially established as a disease diagnostic and various other analytical applications in the future.

Chapter 5 In this chapter; a green synthetic approach was developed for producing fluorescent CQDs by the hydrothermal treatment of *T. indica* leaves for the first time. Furthermore, the synthesized CQDs is prepared without any chemical modification which offers the advantages of cost-effectiveness and effortlessness. This methodology involves zero cost, short reaction time, and ultrapure water as the reaction solvent. There is no need

for additional surface passivating reagents since the *T. Indica* leaves serve as both the carbon precursor and surface passivating agent. The particle size distribution of synthesized CQDs confirmed that the particles were with an average diameter of 3.4±0.5 nm. Their XRD spectrum showed a broad peak at $2\theta = 22^{o}$ which was attributed to the (002) Bragg reflection. The interlayer spacing corresponding to this plane is equal to 0.32 nm which was similar to the graphitic interlayer spacing. Moreover, optical properties of synthesized CQDs were explored. The FTIR analysis revealed the presence of –OH/–NH, C=C, and C=C–NH in an aromatic heterocycling ring. This result was further supported by the XPS analysis. The as-prepared CQDs show excitation dependent behavior in the range 260–400 nm with a high QY of 46.6%. In addition, the prepared CQDs also served as a label-free sensing probe for the detection of Hg^{2+} which exhibits the high sensitivity and selectivity with a LOD as low as 6 nM in a linear range of 0 to 0.1 μM. The proposed sensing system is also effectively used for the analysis of real pond water sample. Therefore, the present approach upwards the scalability in terms of producing bio-compatible CQDs which could be potentially apply in sensing, bio-imaging, disease diagnostics, and other analytical applications.

Chapter 6 In the current chapter, the CQDs was prepared through a simple, green, facile, and single-step hydrothermal treatment by using latexes of medicinal plant *E. milii* for the first time. The proposed method has many advantages such as there is no use of strong concentrated acid which did not release any toxic gases, use of zero-cost green precursor instead of costly organic carbon precursors which avoided the metal contamination, and ultrapure water as a green solvent. This methodology took ultrapure water as a green solvent; avoid the use of strong concentrated acid, and post-surface passivating agents. The TEM micrograph of synthesized CQDs confirmed that particle had an average diameter of 3.4 nm.

The broad XRD peak at $2\theta = 23^{o}$, attributed to the 002 Bragg reflections and the corresponding interlayer spacing along with this plane was equal to 0.32 nm which was comparable with the graphite interplanar spacing. The FTIR spectrum assigned to the C=C–H, C–C–H, C=O, and O=C–NH stretching vibrations, respectively which were further supported by the XPS analysis. The resultant CQDs displayed excellent optical properties including high QY up to 39.2 %, resisted to high salt strength, and longtime photostability. Furthermore, the prepared CQDs served as an intrinsic peroxidase-mimic for catalyzing the TMB in the presence of H_2O_2 at 652 nm. In addition to this, the proposed TMB based system acted as a probe toward the detection of GSH with good selectivity in different amino acids and various other interfering agents. The LOD towards the GSH detection was found to be 5.3 nM in a linear range 0.02-0.1 μM which showed superiority to another reported probe. The proposed TMB based sensing system was successfully applied to the human blood serum samples with good recovery 93.4–102.9 %, which demonstrated the practical feasibility of the present sensing system.

After the extensive literature survey associated to the synthesis of different type of CQDs based on the various organic precursors and completion of the present thesis work, following suggestion might be useful for the production of these CQDs and their applications in future.

- There are large number of investigations that involved in the effective preparation and optimization of CQDs. The hydrothermal method is highly utilized in the synthesis of these CQDs in comparison to other synthesis methods. Nevertheless, there are more avenues to explore in the preparation and optimization of these CQDs via different synthesis protocols in near future.
- Various facile synthetic methods have been used for CQDs preparation, atom-precise and well-defined structures have not been reported yet, which is important for studies on the relationships between structure and properties, precise control of properties, and exploration of new methods and applications.
- In most of the research studies, the reasons behind the enhancement of fluorescence QY in the doped and co-doped CQDs as compared to the normal CQDs are not completely solved. Thus, it should be possible to clearly understand the inherent photoluminescence mechanism in the doped and co-doped CQDs in future. Thus, more theoretical and experimental works and combinations should be expected.
- Furthermore, Most of the as-synthesized doped and co-doped CQDs has emitted blue fluorescence. Hence, the doped and co-doped CQDs with multi-color emission and consequently utilized in different applications in future.

- Moreover, it has been established that the CQDs can be efficiently exploited in wide range of applications counting LED's, solar cells, fluorescent ink, drug delivery, detection of pesticides, temperature probe fungicides, and photocatalysis.